Crisis and enhancement of chaotic scattering

Ying-Cheng Lai[1,2] and Celso Grebogi[2,3]
[1]Department of Biomedical Engineering, The Johns Hopkins University School of Medicine, Baltimore, Maryland 21205
[2]Laboratory for Plasma Research, University of Maryland, College Park, Maryland 20742
[3]Department of Mathematics and Institute for Physical Science and Technology, University of Maryland, College Park, Maryland 20742
(Received 28 December 1993)

Chaotic scattering is characterized by the existence of nonattracting chaotic invariant sets in phase space. There can be several chaotic invariant sets coexisting in phase space when a system parameter value is below some critical value. As the parameter changes through the critical value, stable and unstable foliations of these chaotic invariant sets, which are fractal sets, can become tangent and then cross each other. The first tangency, which provides the linking between chaotic invariant sets, is a crisis in chaotic scattering. Above the crisis, there is an infinite number of such tangencies which keep occurring until the last tangency, above which the stable and unstable foliations cross transversely. As a consequence of this, the fractal dimension of the set of singularities in the scattering function increases in the parameter range determined by the first and the last tangencies. This leads to a proliferation of singularities in the scattering function and, consequently, to an enhancement of chaotic scattering. The phenomenon is investigated by using both simple one-dimensional models and a two-dimensional physical scattering system.

PACS number(s): 05.45.+b, 03.80.+r

I. INTRODUCTION

Chaotic scattering has been found in a variety of physical systems [1–5]. In such a case, the scattering function, which represents the dependence of some output variable characterizing the scattering trajectory after the scattering on some input variable characterizing the trajectory before the scattering, displays a Cantor set of singularities. Hence arbitrarily small changes in the input variable can result in large changes in the output variable. This is the sensitive dependence on initial conditions which gives rise to the term "chaotic scattering." Dynamically, chaotic scattering is due to the existence of some nonattracting chaotic invariant sets in phase space containing an uncountably infinite number of unstable periodic orbits [1–5].

An active area of recent interest is to investigate the appearance and evolution of chaotic scattering as some system parameter changes. Various studies [2–4] have revealed two basic routes to chaotic scattering. One is the abrupt bifurcation route in which a chaotic invariant set is suddenly formed in the phase space as some parameter varies through a critical value [2]. The other is the period-doubling bifurcation route in which a chaotic invariant set is gradually formed from a saddle-center bifurcation [3]. Besides these two routes, transition to chaotic scattering can also arise as a discontinuity in the grammatical complexity and hence in the topological entropy resulting from the onset of a devil's staircase [6]. Studies also reveal that after the onset of chaotic scattering, further qualitative changes in the chaotic invariant set are possible as the system control parameter changes [3,4] and those changes may result in qualitative, physically noticeable changes in the scattering function. One example is the so-called massive bifurcation [4] in which an infinite number of unstable periodic orbits in the chaotic invariant set is suddenly destroyed and simultaneously replaced by another class of infinite number of unstable periodic orbits.

In this paper, we present a new phenomenon in chaotic scattering. It is akin to the merging crisis [7] in dissipative chaotic systems. We henceforth call this phenomenon *crisis in chaotic scattering* [8]. Chaotic scattering occurs on both sides of the crisis. Before the crisis, there exist two *topologically and dynamically isolated* chaotic invariant sets in the phase space. As a system parameter changes, the closures of the stable and unstable manifolds of the two chaotic sets first touch each other at the crisis. Since both stable and unstable foliations have Cantor structures, as the parameter is varied further, both foliations pass through each other experiencing an uncountably infinite number of heteroclinic tangencies in the process. The initial tangency, then, corresponds to the crisis and provides the linking between the two chaotic invariant sets.

There are two major consequences resulting from this crisis. The first one is that once the crisis has occurred, an uncountably infinite number of new periodic and chaotic trajectories are suddenly created. These trajectories live in the union of the two chaotic sets that existed before the crisis. However, as long as the stable and unstable foliations keep creating tangencies as the parameter varies, the number of periodic and chaotic trajectories keeps increasing. It means that there is an uncountably infinite number of new possibilities for scattering trajectories. The second major consequence is that the fractal dimension of the set of singularities in the scattering function increases after the crisis. We stress that these consequences are caused by an uncountably infinite number of tangencies of stable and unstable foliations, which

occur when both foliations have a fractal structure. Such Cantor-like stable and unstable foliations are, however, typical in chaotic scattering systems [1–5].

Our approach will be to investigate a class of simple one-dimensional systems for which the phenomenology of crisis in chaotic scattering can be understood fairly completely. We then study a physical scattering system which consists of an infinite array of two-dimensional, nonoverlapping, stationary, and circular potential wells. By choosing an appropriate, physically realizable form for the potential, this system exhibits the crisis phenomenon. The physical mechanism for the crisis in this scattering system is also investigated.

The organization of the paper is as follows. In Sec. II we introduce and analyze a class of simple one-dimensional models. In Sec. III we describe a physical scattering system and present numerical results. In Sec. IV we present discussions.

II. ONE-DIMENSIONAL MODELS

We consider the following two-parameter family of one-dimensional map:

$$f_b(x)=\begin{cases}-a|x+1|+b, & x\le 0\\ a|x-1|-b, & x>0\end{cases}, \tag{1}$$

where $x\in\mathbb{R}$ and a and b are parameters ($b>-1$). The map is invariant under the following symmetrical operations: $x\to -x$ and $f_b(x)\to -f_b(x)$. For small values of a, the map can exhibit bounded attractors, while for large a values, almost all initial conditions except a set of measure zero asymptote to either ∞ or $-\infty$. Since we are interested in modeling a situation of scattering where particles eventually escape to $\pm\infty$, we will fix a at a reasonably large value and investigate the dynamical behavior of the map as b is increased from zero. As shown in Fig. 1(a), there are two intervals $A_+\equiv[-x_b,-x_a]$ and $A_-\equiv[x_a,x_b]$ determined by the fixed points on the two branches of the map with positive slope. For initial conditions outside these intervals, the resulting trajectories asymptote to either ∞ or $-\infty$ without entering the two intervals. The values of x_b and x_a are determined by the following relations: $a(x_b-1)-b=x_b$ and $a(1-x_a)-b=x_b$. We have

$$x_b=\frac{a+b}{a-1},\quad x_a=\frac{a-b-2}{a-1}. \tag{2}$$

To ensure that almost all initial conditions asymptote to $\pm\infty$, we require that $x_a>0$, or equivalently

$$a\ge(b+2). \tag{3}$$

Depending on the value of b, Eq. (1) exhibits different dynamical behavior. In particular, when $f_b(1)>x_a$, there are attractors in the intervals A_+ and A_-. Initial conditions inside A_+ and A_- asymptote to the respective attractors. When $f_b(1)<x_a$, i.e., $a>2$, almost all initial conditions in A_+ and A_- escape to ∞ except two Cantor sets of Lebesgue measure zero. In this case, when one initial condition asymptotes to $+\infty$ ($-\infty$), a slightly perturbed one may asymptote to $-\infty$ ($+\infty$) and hence the dynamics are similar to these of chaotic scattering. When $f_b(1)>-x_a$, as shown in Fig. 1(a), the Cantor sets in A_+ and A_- are topologically and dynamically isolated. Trajectories resulting from initial conditions in A_+ cannot enter A_- and vice versa. Due to the symmetry, the fractal dimensions of these two Cantor sets are the same. The dimension is $d_1=\ln 2/\ln a$, which can be seen as follows. Consider the interval A_+. At the first iteration, initial conditions in the interval $G_+=(x_a+S_f,x_b-S_f)$ map outside A_+ and approach either ∞ or $-\infty$ in subsequent iterations, where $S_f=2(b+1)/a(a-1)$. Hence there are two line segments of length S_f that stay in A_+ after the first iteration. Two inverse images of G_+ on each side of G_+ map out of A_+ in two iterations and hence there are four intervals within A_+ of length S_f/a that can stay in A_+ for two iterations. In general, there are 2^n intervals of length S_f/a^{n-1} that can survive n iterations. Therefore, the box-counting dimension [9] of the Cantor set is

$$d_f=-\lim_{n\to\infty}\frac{\ln 2^n}{\ln(S_f/a^{n-1})}=\frac{\ln 2}{\ln a}. \tag{4}$$

A crisis occurs when $f_b(+1)=-x_a$ or $b_f=(a-2)/a$, after which the two Cantor sets in A_+ and A_- are heteroclinically connected to each other, as shown in Fig. 1(b). This is an heteroclinic tangency analogous to that of stable and unstable manifolds in two-dimensional maps. As b increases beyond b_f, there can be an infinite number of such tangencies determined by the Nth-fold of the map $f_b^{(N)}(x)\equiv f_b(f_b(\cdots f_b(x))\cdots)$, where integer $N>2$. The last tangency occurs when $f_b(+1)=-x_b$ or $b_l=a/(a-2)$, as shown in Fig. 1(c). For $b\ge b_l$, there is a single Cantor set in the interval $A_t\equiv[-x_b,x_b]$. The dimension of this Cantor set can be computed referring to Fig. 1(d). Initial conditions in $(-x_a,x_a)$ maps outside A_t in one iteration. In addition, there are open intervals $G_1=(-x_b+S_l,-x_a-S_l)$ and $G_2=(x_a+S_l,x_b-S_l)$ that maps outside A_t in one iteration, where $S_l=2(a+b)/[a(a-1)]$. After the first iteration, there are four intervals of length S_l that survive in A_t for one iteration. The preimages of these four intervals consist of 16 subintervals of length S_l/a which stay in A_t for 2 iterations. In general, there are 4^n intervals of length S_l/a^{n-1} that survive in A_t for n iterations. Thus the dimension of the Cantor set is

$$d_l=-\lim_{n\to\infty}\frac{\ln 4^n}{\ln(S_l/a^{n-1})}=2\frac{\ln 2}{\ln a}. \tag{5}$$

Note that in order for d_l to be less than one, it is required that $a>4$; otherwise $d_l=1$ and there will be attractors in A_t. The condition $a>4$ is guaranteed by Eq. (2), which when combined with $b_l=a/(a-2)$ gives the same constraint for a.

Equations (4) and (5) thus indicate that the fractal dimension of Cantor sets increases from $\ln 2/\ln a$ to $2\ln 2/\ln a$ as b increases from values less than b_f to values greater than b_l. The value of d, as we have seen above, is determined by behavior of $f_b(x_c)$, where $x_c=\pm 1$ are the two critical points of the map. For $b_f<b<b_l$, the value

of d is determined by higher iterates of the critical points as explained next. Consider, for example, $f_b^{(2)}(+1)$. When

$$-x_a < f_b^{(2)}(+1) < x_a \ , \tag{6}$$

there are no new tangencies and hence d remains at constant values. Tangencies occur when $f_b^{(2)}(+1) = \pm x_a$. There are two parameter intervals determined by $f_b^{(2)}(+1) = \pm x_a$ in which d is a constant. These intervals are $[b_l^1, b_f^1]$ and $[b_l^2, b_f^2]$, where

$$b_l^1 = \frac{2a - 2 - a^2}{2 - a^2}, \quad b_f^1 = \frac{a^2 - 2}{a^2} \ ,$$
$$b_l^2 = \frac{a^2 + 2 - 2a}{a^2 - 2a}, \quad b_f^2 = \frac{a^2 - 2}{a^2 - 2a + 2} \ . \tag{7}$$

Plots of $f_b^{(2)}(x)$ at these four values of b are shown in Figs. 2(a)–2(d), respectively. It is clear that tangencies occur at all these b values. In particular, b_l^1 and b_l^2 correspond to two "last" tangencies of the map $f_b^{(2)}(x)$, while b_f^1 and b_f^2 correspond to two "first" tangencies. The plateau dimension values within these two intervals, however, are difficult to compute analytically because there are

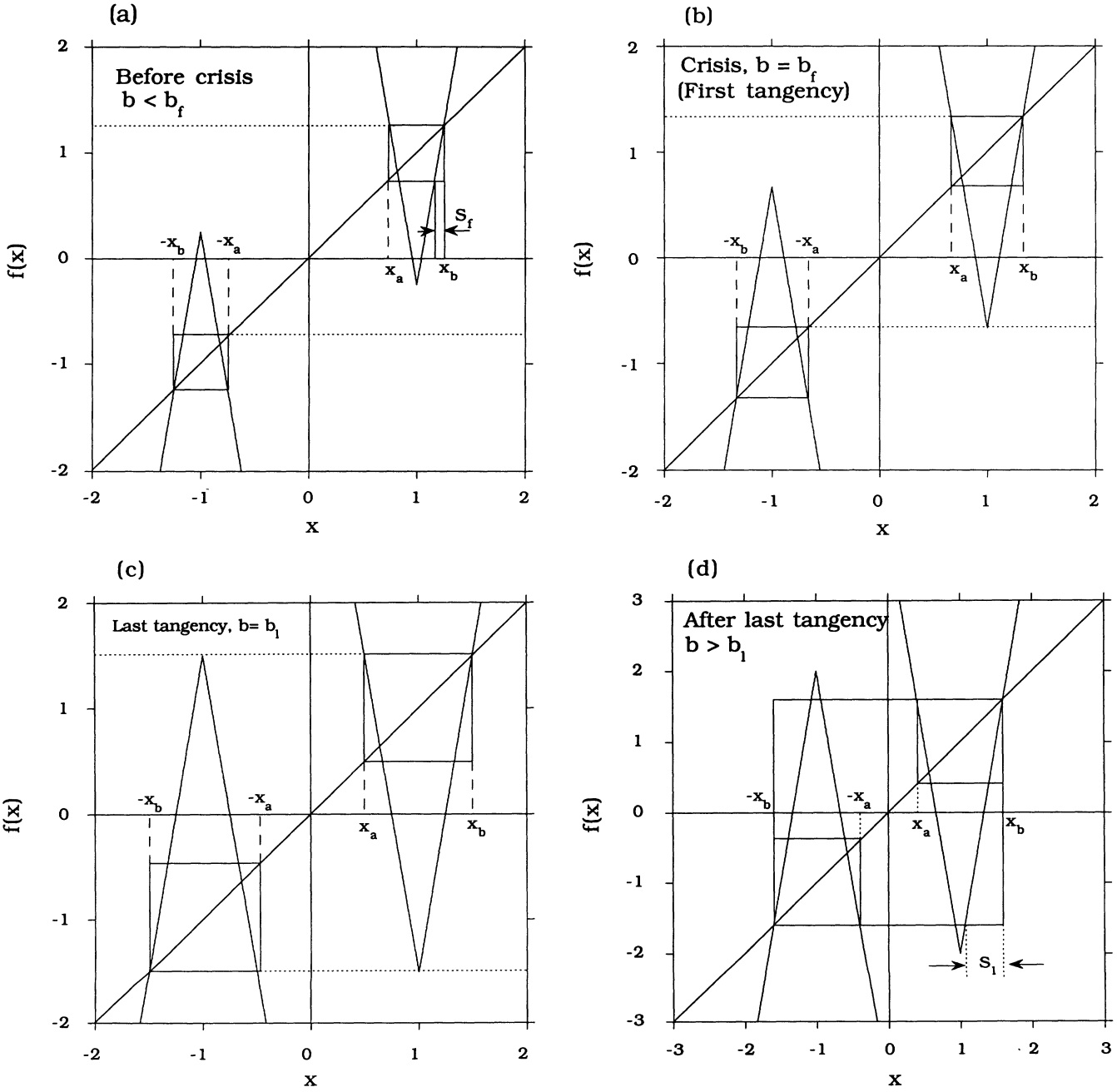

FIG. 1. The one-dimensional model Eq. (1) (a) before crisis, (b) at the crisis (first tangency), (c) at the last tangency, and (d) after the last tangency.

other peaks of $f_b^{(2)}(x)$ function appeared inside the squares determined by $\pm x_a$ and $\pm x_b$, as shown in Figs. 2(a)–2(d).

Similarly, in parameter ranges where d increases, there are six even smaller intervals determined by $-x_a < f_b^{(3)}(+1) < x_a$ in which d remains constant values. These observations imply that there is *an infinite number* of parameter subintervals within which d remains constants. The increment of d occurs at the closure of the set of parameter values corresponding to tangencies determined by $f_b^{(n)}(\pm 1)$, $n = 1,2,\ldots,\infty$. There are an infinite number of such tangencies. This leads to the function $d(b)$ for $b_f \le b \le b_l$ being a devil's staircase.

The above argument leading to the assertion that $d(b)$ is a devil's staircase function is not rigorous. To verify this, we have numerically computed the function $d(b)$ for $a = 6$ and $0.25 < b < 2.0$. For this a value, we have $b_f = \frac{2}{3}$ and $b_l = \frac{3}{2}$. For $b < b_f$, $d = \ln 2/\ln 6 \approx 0.38$. For $b > b_l$, $d = \ln 4/\ln 6 \approx 0.78$. For $b_f < b < b_l$, there are two intervals determined by Eq. (7) in which d takes values between ln2/ln6 and ln4/ln6. These two intervals are [13/17,17/18] and [13/12,17/13]. To compute d, we use

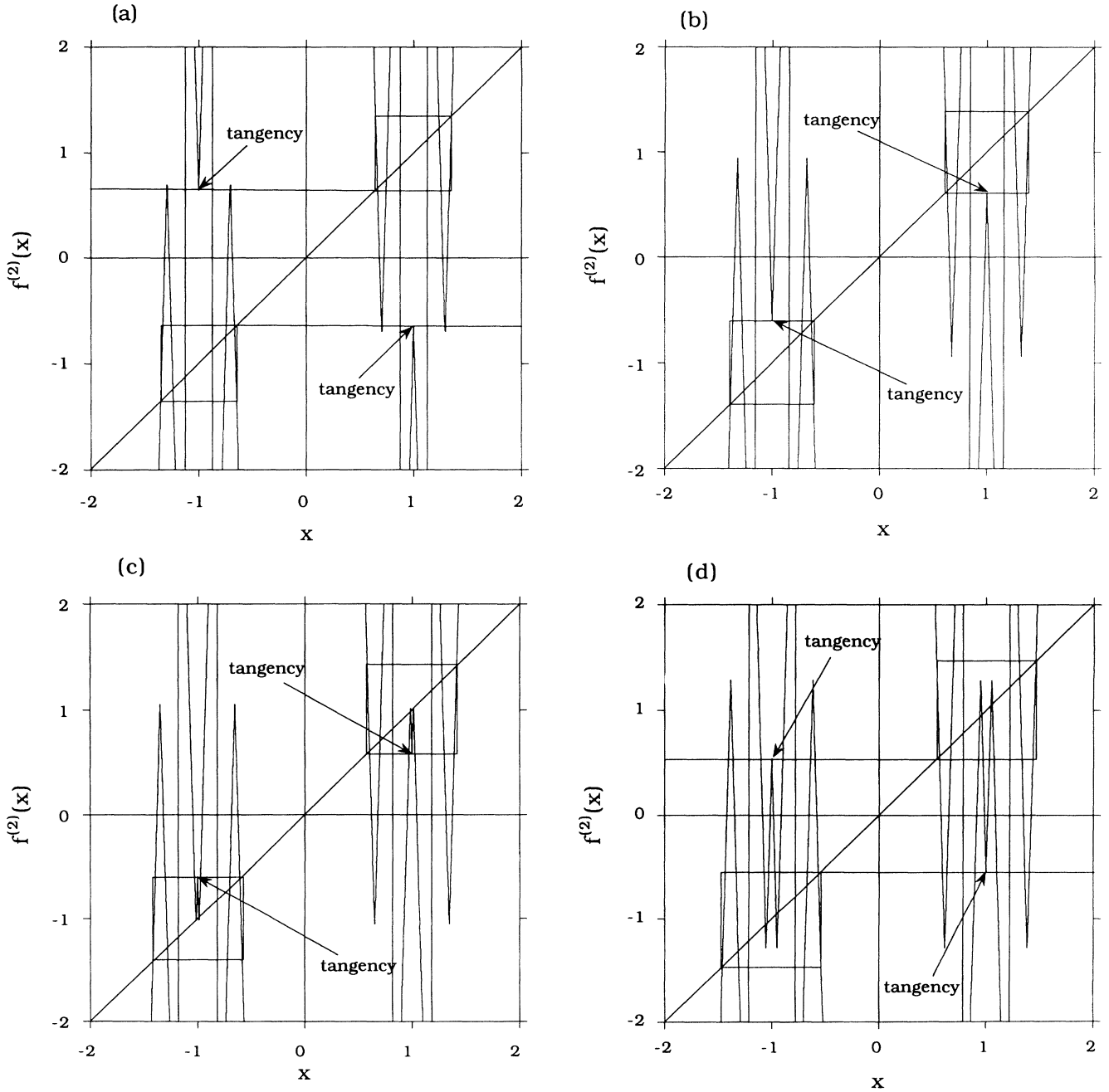

FIG. 2. Second iterate of the one-dimensional model Eq. (1) at (a) $b = b_l^1$, $f_b^{(2)}(+1) = -x_a$; (b) $b = b_f^1$, $f_b^{(2)}(+1) = x_a$; (c) $b = b_l^2$, $f_b^{(2)}(+1) = -x_a$; and (d) $b = b_f^2$, $f_b^{(2)}(+1) = x_a$. In both the intervals $[b_l^1, b_f^1]$ and $[b_l^2, b_f^2]$, the fractal dimension of the Cantor set remains constant.

the uncertainty algorithm originally proposed to calculate dimension for fractal basin boundaries arising in dynamical systems that possess multiple attractors [10]. The procedure is as follows. For a given b value, we randomly choose an initial condition $x_0 \in [-2,2]$. This initial condition is then perturbed to yield another initial condition $x_0+\epsilon$, where the perturbation ϵ is small. The asymptotic state of these two initial conditions are then computed by iterating Eq. (1). In particular, if one initial condition leads to a trajectory that asymptotes to ∞ and another to $-\infty$, then the initial condition x_0 is said to be uncertain. For given perturbation ϵ, the fraction of uncertain initial conditions $F(\epsilon)$ is obtained by accumulating 200 (in our computation) uncertain initial conditions. In general, $F(\epsilon)$ scales with ϵ as $F(\epsilon) \sim \epsilon^{\alpha}$, where α is the uncertainty exponent [10]. The dimensions of the Cantor set is given by $d=1-\alpha$, which is equal to the box-counting dimension for one-dimensional dynamical systems [11]. Figure 3 shows the computed $d(b)$ curve which contains values of d for 700 values of b uniformly chosen in [0.25,2.0]. The dimension values for $b < b_f$ and $b > b_l$, as well as the two largest subintervals of b in which d is constant, agree with our theoretical predictions Eqs. (4), (5), and (7). The two plateau dimension values within the subintervals are approximately 0.56 and 0.68. Plateau dimension values determined by high iterates of the map are difficult to see due to numerical resolution.

The feature in which the fractal dimension maintains constant values for a dense set of parameter intervals in which no tangency occurs is specific to Eq. (1). When the form of the map is changed, the dimension can change even when there is no tangency. In particular, for quadratic maps (slope is zero at critical points), the dimension can decrease in parameter intervals where there is no tangency, although there is an overall dimension increase when the parameter changes from the crisis value to the last tangency value. To illustrate this, we consider the

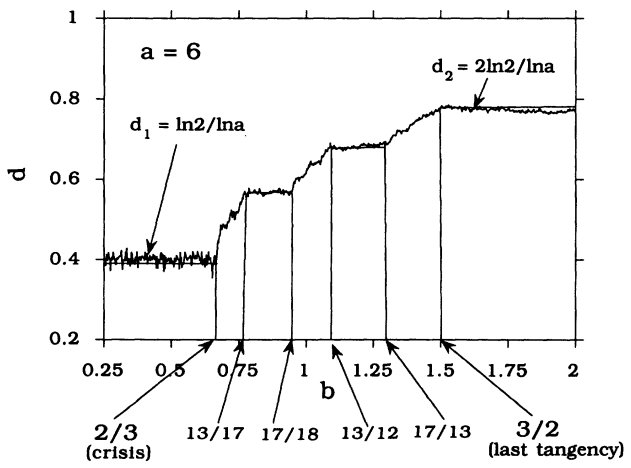

FIG. 3. The fractal dimension of the Cantor set versus the parameter b in $b \in [0.25,2.0]$, where $a=6$ is fixed in Eq. (1). This crisis occurs at $b_f=2/3$ and the last tangency occurs at $b_l=\frac{3}{2}$. For $b < b_f$, $d=\ln 2/\ln a$. For $b > b_l$, $d=2\ln 2/\ln a$. The function $d(b)$ for $b_f \le b \le b_l$ is apparently a devil's staircase.

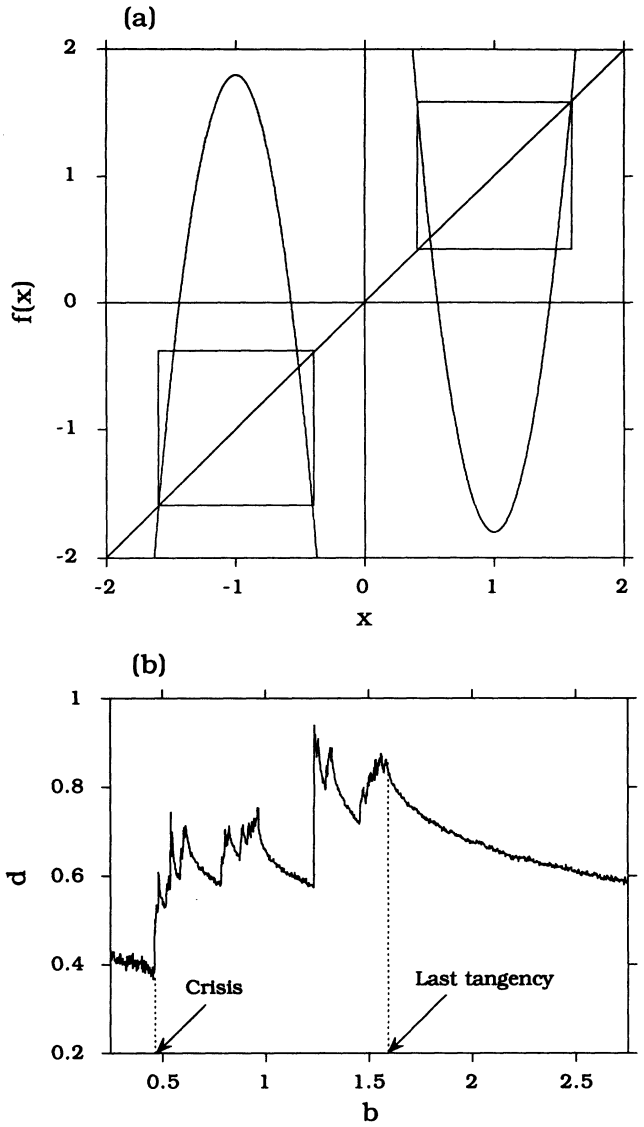

FIG. 4. (a) A quadratic map Eq. (8). (b) The fractal dimension versus the parameter b. In contrast to the tent map in Eq. (1) in which the dimension of the Cantor set exhibits an infinite number of plateau values for $b_f \le b \le b_l$ when there is no tangency, the dimension can decrease for the quadratic family of Eq. (8) in parameter intervals where there is no tangency.

following two-parameter family of quadratic map, as shown in Fig. 4(a):

$$g_b(x)=\begin{cases} -(2a+b)(x+1)^2+b, & x \le 0 , \\ (2a+b)(x-1)^2-b, & x>0 , \end{cases} \tag{8}$$

where $a=6$. Figure 4(b) shows the curves $d(b)$ in a parameter range containing the crisis and the last tangency. We stress, however, that the dimension does increase when tangencies occur. This feature is independent of the particular map.

III. A PHYSICAL SCATTERING SYSTEM

In this section we demonstrate the phenomenon of crisis in chaotic scattering in an open Hamiltonian sys-

tem. This system was originally introduced by Troll and Smilansky [5]. Figure 5 schematically shows the model system in which a point particle is scattered by an infinite array of two-dimensional elastic scatterers. These scatterers are placed in the plane at constant intervals D along the y axis. Each scatterer is represented by a circular potential $V(r)<0$ that becomes negligible for $r>R$, where $R<D/2$ (nonoverlapping condition). The nonoverlapping condition means that particle trajectories are straight lines in regions between adjacent potentials. If $V(r)>0$ (repulsive), only trivial invariant orbits can be formed in the potential region and hence the dynamics are simple and not interesting. The effect of each individual scatterer on a scattering trajectory can be characterized by the elastic deflection angle $\theta(l)$, which is a function of the angular momentum l, as shown in Fig. 5. Simple classical mechanics gives

$$\theta(l)=\pi-\sqrt{2}l\int_{r_t}^{\infty}\frac{dr}{r^2\sqrt{E-V(r)-l^2/2r^2}}\ , \tag{9}$$

where E is the particle energy. The mass of the particle is assumed to be unit, and r_t is the radius at the turning point of scattering trajectories determined by the following equation:

$$E-V(r_t)-\frac{l^2}{2r_t^2}=0\ . \tag{10}$$

Note that $\theta(l)<0$ for $l>0$. Since the system is invariant under time reversal, we have $\theta(-l)=-\theta(l)\mathrm{mod}(2\pi)$. Due to the finite range of each scatterer, $\theta(l)=0$ for $l>l_{\max}=uR$, where u is the particle velocity in the region where the potential is negligible. For a particle moving towards a scatterer with angular momentum l and velocity $\mathbf{u}$, its new velocity $\mathbf{u}'$ after scattering has the same magnitude as $\mathbf{u}$, but has a different direction. Let β and β' be the angles measured counterclockwisely that $\mathbf{u}$ and $\mathbf{u}'$ make with respect to the $-y$ axis, respectively. Then from Fig. 5 we have

$$\beta'=\beta+\theta(l)\ . \tag{11}$$

After this deflection, the particle may either collide with the scatterer above (if $u_y'=-\cos\beta'>0$) or enter the scatterer below (if $u_y'<0$). In either case, scattering is determined by the value of angular momentum l' relative to the new scatterer. Simple geometrical argument from Fig. 5 leads to the following expression for l':

$$l'=l+(Du)\mathrm{sgn}(\cos\beta')\sin\beta'\ . \tag{12}$$

If $|l'|\geq l_{\max}$, the particle continues to move along a straight line trajectory leaving the array of scatterers and never returns. Such particles will be regarded as having escaped from the scattering region. New scattering occurs only if $|l'|<l_{\max}$. Following Troll and Smilansky [5], we choose β and l as our dynamical variables. Thus the two-dimensional map Eqs. (11) and (12) can be symbolically represented as

$$(\beta',l')=M(\beta,l)\ . \tag{13}$$

The phase space for M is defined by the domain $[0,2\pi)\times[-l_{\max},l_{\max}]$, which is a cylinder. It can be easily verified that M is area preserving.

In our subsequent numerical experiments, we choose $V(r)$ to be the following Woods-Saxon potential [12] which is often used in the context of nuclear physics [13]:

$$V(r)=\frac{-V_0}{1+\exp[(r-R_0)/\alpha]}\ , \tag{14}$$

where V_0 (>0), R_0, and α are constants. At large distance r, $V(r)$ behaves like the Yukawa potential that vanishes exponentially as r increases. We fix $V_0=10$, $R_0=0.5$, $\alpha=0.1$, $D=4$, and $R=1.4$. Thus $V(r=R)/V_0\sim10^{-4}$, so in practice adjacent potentials do not overlap each other. When the particle energy is large, say $E\gg10$, we observe that the phase space contains Kol'mogorov-Arnol'd-Moser (KAM) surfaces and chaotic regions [14] (nonhyperbolic chaotic scattering). For $E<10$, we find numerically that all the KAM surfaces are destroyed and the phase space only contains chaotic invariant sets (hyperbolic chaotic scattering). Henceforth we choose E as our control parameter and investigate the scattering behavior of the system for $E<10$.

The chaotic invariant sets lie in the closure of the intersection of the stable and unstable manifolds. Note that the map has two unstable fixed points: $(0,0)$ (corresponding to a straight trajectory along the $-y$ axis) and $(0,\pi)$ (corresponding to a straight trajectory along the $+y$ axis). Numerically, we find that for $E>E_f\approx4.4$, there exist two *topologically and dynamically isolated* chaotic invariant sets associated with these unstable fixed points. Note that the two chaotic sets must be identical due to the symmetry of the system with respect to $\beta=0$ (or 2π) and $\beta=\pi$. At the energy value $E_f\approx4.4$, the stable manifold of one chaotic set becomes heteroclinically tangent to the unstable manifold of the other chaotic set, as shown in Fig. 6(a). At this crisis point, both chaotic sets

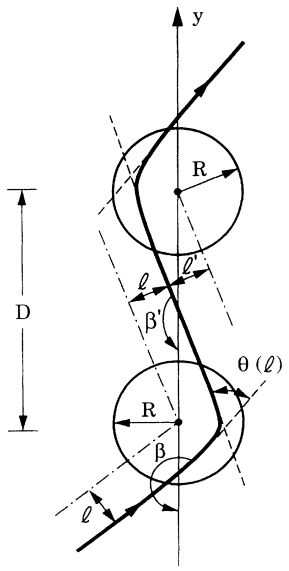

FIG. 5. The Troll-Smilansky scattering system in which particles interact with an infinite array of two-dimensional, nonoverlapping, and circular potential wells. The dynamical variables are angle β and angular momentum l.

are dynamically linked and particles initiated near one chaotic set can reach and exit along the unstable manifold of the other chaotic set. As E decreases passing through E_f, the closures of the stable and unstable manifolds of the two chaotic sets heteroclinically cross each other forming additional chaotic sets at the intersection. Since both the stable and unstable foliations of the chaotic sets have Cantor structures before the crisis, there must be an uncountably infinite number of tangencies between E_f and $E_l \approx 4.1$ [corresponding to the last tangency, as shown in Fig. 6(b)].

It is known that Cantor structures in stable and unstable foliations give rise to an infinite number of singularities in the scattering function [1–5]. For our system it is convenient to define a scattering function as the exit angle β_{out} versus the incoming angular momentum l of a particle trajectory at fixed incident angle β_{in}. (The angular momentum is related to the impact parameter s by $l = us$.) Figures 7(a) and 7(b) show the scattering functions at $E = 5$ (before the crisis) and $E = 1$ (after the crisis), respectively. Both plots exhibit the typical feature of chaotic scattering [1–5]. That is, they contain both smooth parts and wildly oscillating parts. Further enlargements of these plots in the oscillating regions reveal similar structures. Moreover, the exit angle β_{out} at $E = 1$ can have any values between 0 and 2π. This means that an upward incident trajectory ($\pi/2 \le \beta_{\text{in}} = 2.55 < 3\pi/2$) can turn over, possibly cycle in some potential, and then exit downward ($0 \le \beta < \pi/2$ or $3\pi/2 \le \beta < 2\pi$) for $E = 1$. Due to the symmetry of the system (the system is invariant under $\beta \to \beta + \pi$), a downward moving trajectory can exit upward. However, at large energy ($E > 5$), we observe numerically that an upward (downward) incident particle can never exit downward (upward). This means that as E is decreased, the deflection angle of a particle trajectory caused by an individual scatterer increases substantially, enabling the particle trajectory to turn over and cycle in the individual potential. Comparison between Figs. 7(a) and 7(b) indicates that there appear to be "more" singularities at $E = 1$ than at $E = 5$, which suggests that the scattering is enhanced after the crisis.

We now compute the fractal dimension of the set of singularities in the scattering function as the energy value is decreased passing the crisis value. The procedure is similar to that used to obtain Figs. 3 and 4(b). Briefly, for a fixed value of "uncertainty" ϵ, we randomly choose an

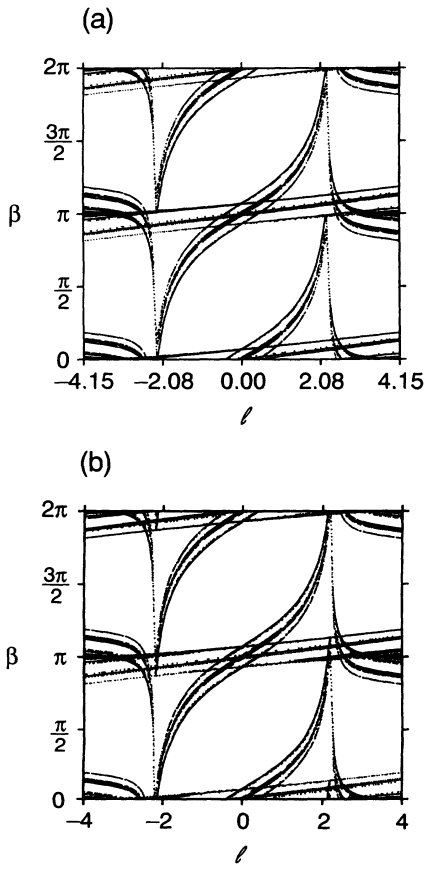

FIG. 6. Stable and unstable foliations for (a) $E = 4.4$ (near the crisis) and (b) $E = 4.1$ (near the last tangency). The unstable foliation is nearly horizontal.

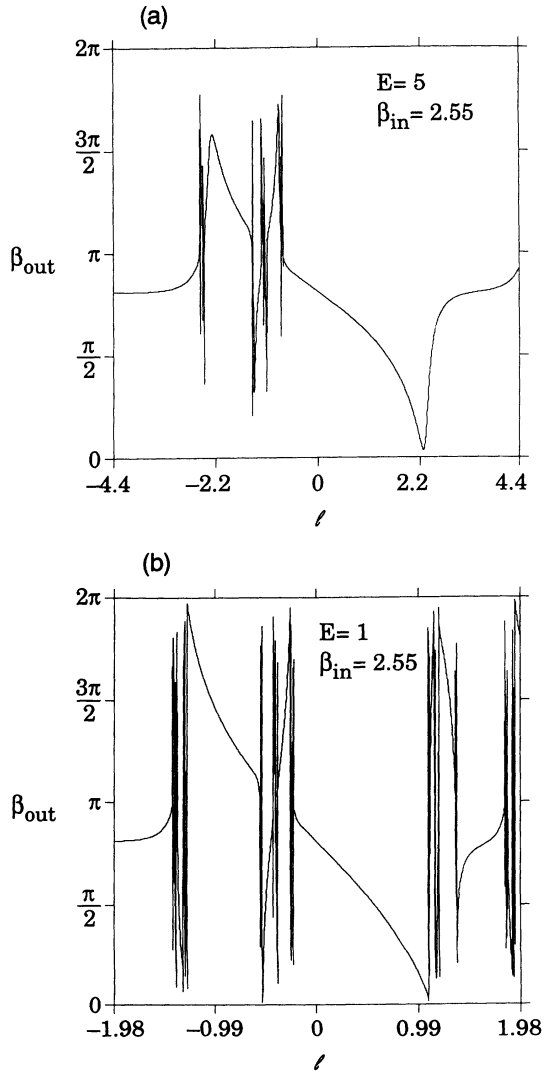

FIG. 7. Scattering functions for (a) $E = 5$ and (b) $E = 1$. The incident angle is $\beta_{\text{in}} = 2.55$. Note that visually there appear to be "more" singularities in the scattering function at $E = 1$.

initial condition l_0 at some fixed value of β_{in} (2.55 in our computation) and two other initial conditions $l_0 \pm \epsilon$. The initial condition l_0 is said to be uncertain if these three initial conditions exit the system via different scatterers. Figures 8(a) and 8(b) show plots of the uncertainty fraction $f(\epsilon)$ (computed by accumulating the number of uncertain initial conditions to 200) versus ϵ on a logarithmic scale for $E=5$ and 1, respectively. These data can be fitted by straight lines, the slopes of which give the uncertainty exponent α ($\alpha=0.53\pm0.02$ for $E=5$ and $\alpha=0.43\pm0.01$ for $E=1$). Fractal dimensions of the Cantor sets in the scattering function are therefore $d(E=5)=0.47\pm0.02$ and $d(E=1)=0.57\pm0.01$. Figure 9 plots d versus E, which shows that $d\approx0.486$ for

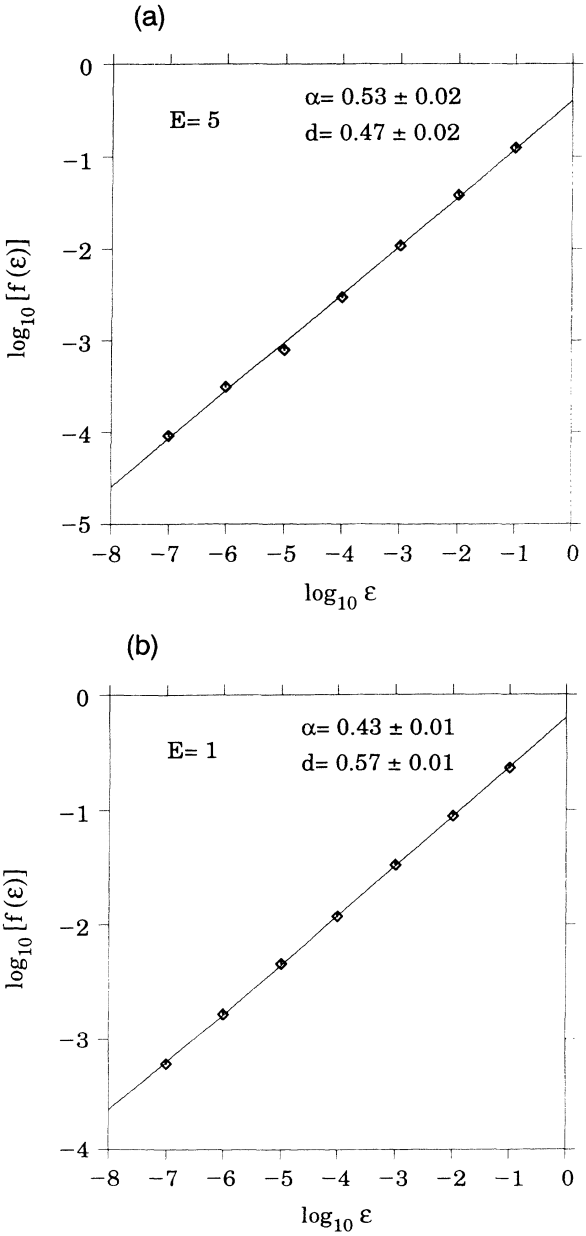

FIG. 8. Uncertainty fraction $f(\epsilon)$ versus ϵ on a logarithmic plot for (a) $E=5$ and (b) $E=1$. The uncertainty exponent α is the slope of the plot and the uncertainty dimension is given by $d=1-\alpha$.

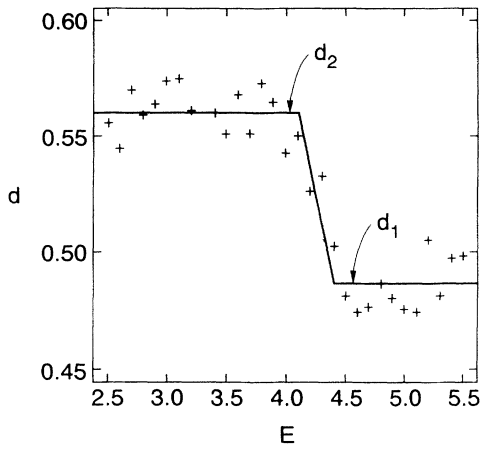

FIG. 9. Fractal dimension of the set of singularities of the scattering function as a function of E obtained by fixing $\beta_{in}=2.55$.

$E>E_f$. The dimension increases as E decreases from E_f to $E_l\approx4.1$. For $E<4.1$, $d\approx0.560$. The increase in the fractal dimension indicates a proliferation of singularities in the scattering function. Consequently, chaotic scattering is enhanced after the crisis. While there is an overall dimension increase as E decreases from E_f to E_l, the behavior of d in $E_f>E>E_l$ is likely to be very complicated. It is possible that the function $d(E)$ is a devil's staircase in this energy interval, as suggested by the one-dimensional models in Sec. II. Changing β_{in} will not significantly change the dimension values in Fig. 9, as long as the line cuts through all components of the stable foliations. This has been verified by computing the dimension at various energy values with sightly different β_{in}. The overall features of Fig. 9 appear therefore to be robust.

The physical origin of the crisis can be related to the occurrence of "orbiting" of particle trajectories as the energy is decreased. For a circular potential, orbiting means that at a fixed energy value, it is possible for the particle with the critical angular momentum l_{crit} to exhibit near zero radial motion in the potential and hence the particle circulates in the potential for an infinite number of times. Orbiting occurs when both the energy and angular momentum satisfy the following equations:

$$dr/dt|_{r=r_{crit}}=\sqrt{2[E-V_{eff}(r_{crit})]}=0\ ,$$
$$dV_{eff}(r)/dr|_{r=r_{crit}}=0\ , \tag{15}$$

where $V_{eff}(r)\equiv V(r)+l^2/2r^2$ is the effective potential. The latter condition distinguishes orbiting from a turning point of a particle trajectory, which only requires $dr/dt=0$. Figure 10(a) shows an orbiting situation at $E=1$ in which we plot $V_{eff}(r)$ at $l=l_{max}$, $l=l_{crit}\approx1.35$ (the orbiting angular momentum), and $l=0.5<l_{crit}$. For $l=l_{crit}$, $V_{eff}(r)$ attains a local quadratic maximum at $r=r_{crit}$ whose value is equal to the particle energy E. Hence $\theta(l)\to-\infty$ for $l\to l_{crit}$. For values of angular momenta in the neighborhood of l_{crit}, deflection angles are

no longer $-\infty$ but still assume large absolute values. Therefore, for $E=1$, particles with their angular momenta near l_{crit} will circulate in an individual potential for many times before they exit this potential. Figure 10(b) shows $V_{eff}(r)$'s at ten different angular momenta with $l=nl_{max}/10$, where $n=1,2,\ldots,10$ for $E=5$. There exist no values of angular momentum such that the effective potential can exhibit a local maximum at $E=5$ and hence orbiting is not possible for $E=5$. This indicates that deflection angles for scattering particles are small. Consequently, at this energy value particles incident from below (above) can exit only upward (downward), thereby leading to the two isolated chaotic invariant sets being isolated. As the energy is lowered towards the situation of orbiting, the maximum deflection angle θ_{max} increase. When θ_{max} far exceeds π, particle trajectories can turn around so as to induce the crisis observed. Since the occurrence of crisis does not require θ_{max} to be ∞, crisis occurs at an energy value larger than that required for orbiting to occur.

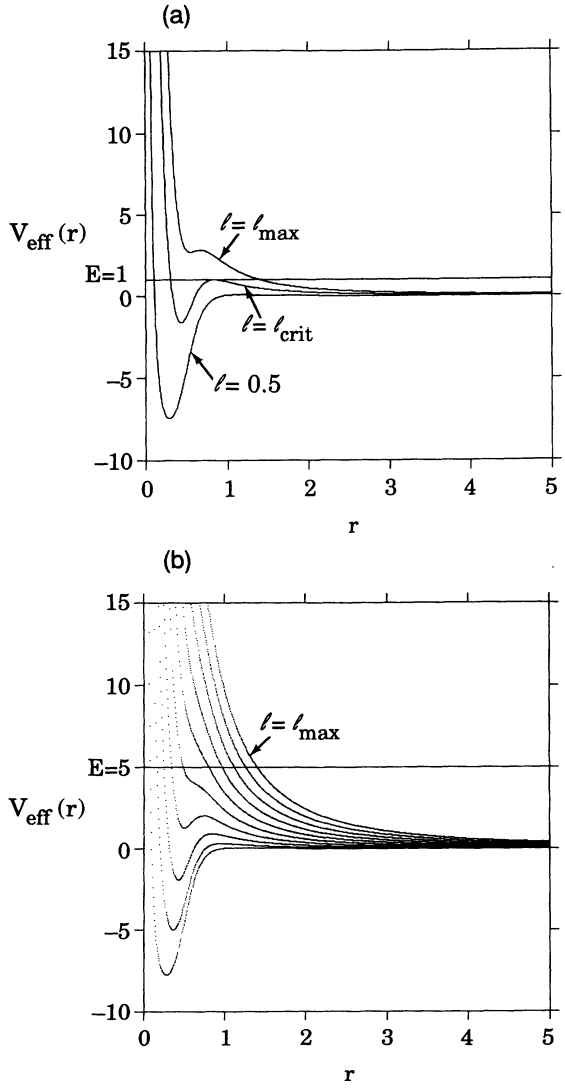

FIG. 10. Plots of $V_{eff}(r)$ at several different angular momenta for (a) $E=1$ and (b) $E=5$. In (a), where orbiting can occur, three $V_{eff}(r)$'s at $l=0.5$, l_{crit} (the orbiting angular momentum), and l_{max} are plotted. In (b), where there is no orbiting, ten $V_{eff}(r)$'s at $l=nl_{max}/10$, $n=1,2,\ldots,10$ are plotted.

IV. DISCUSSIONS

In this paper we have used both one-dimensional models and a two-dimensional physical scattering system to demonstrate the phenomenon of crisis in open dynamical systems that exhibit chaotic scattering. This novel bifurcation in chaotic scattering is characterized by heteroclinic tangencies of stable and unstable foliations of symmetric chaotic invariant sets. The physical manifestation of such crisis is an increase of the fractal dimension in the Cantor set of singularities in the scattering function. Consequently, chaotic scattering is enhanced due to the crisis.

The generality of the phenomenon of crisis in chaotic scattering is suggested by the simple one-dimensional models in Sec. II. While the stable and unstable manifolds associated with the chaotic invariant sets in the two-dimensional physical scattering system look rather special, namely, the stable manifolds have a sharp bend and the unstable manifolds are almost straight, the condition for a crisis to occur is independent of these specific geometrical shapes of the manifolds. As we have discussed in the one-dimensional models, crisis and the subsequent increase in the fractal dimension *depend only on the occurrence of an infinite number of heteroclinic tangencies of the stable and unstable foliations.* Since fractal stable and unstable foliations are a general feature of chaotic scattering systems [1–5], we expect crisis in chaotic scattering to be typical.

The map for the scattering system is smooth and two dimensional. Nonetheless, our one-dimensional models capture the essential features of the two-dimensional scattering system. For instance, although the tangencies are quadratic for the scattering system, the stable manifold exhibits a very large curvature at the tangency. Both stable and unstable manifolds away from the tangency points are almost straight lines. Therefore our one-dimensional model Eq. (1) is a good dynamic representation of the scattering system at the heteroclinic crossing. Furthermore, the one-dimensional models suggest that the function of d versus some parameter value is a devil's staircase in a parameter range determined by the crisis and the last tangency. It is, however, difficult to quantify this explicitly for our two-dimensional scattering model because of the difficulty in computing the uncertainty dimension, which involves numerical integration of deflection angles $\theta(l)$.

At a first glance, the two-dimensional scattering system studied in this paper is very close to the model extensively studied by Troll and Smilansky [5]: Both systems consist of a one-dimensional array of two-dimensional scatterers and individual scattering potentials at lattice sites are radially symmetric and of finite range. But while Troll and Smilansky study the case of a schematic deflection function, linear in the angular momentum,

$$\theta(l)=\begin{cases} kl/(uD), & l\le uR\ , \\ 0, & l>uR\ , \end{cases} \tag{16}$$

we use a realistic scattering potential of the Woods-Saxon type. The linear deflection function in Eq. (16) is a good choice because it enables a detailed analytical analysis of chaotic scattering and the study of various types of bifurcations that lead to chaotic scattering. Our potential is not so readily amenable to analytical investigation, but has the advantage of realistically capturing the energy dependence of quantum phase shifts [14] and classical scattering functions. Moreover, the Woods-Saxon potential, as shown in Sec. III, shows new dynamical phenomena not present in the schematic model studied in Ref. [5]. Nevertheless, the transition to chaotic scattering studied as a function of k in the Troll-Smilansky model (the TS model) serves as a convenient framework in which we will now discuss similarities and differences between the two models.

For small k, $0<k<4$, the TS model exhibits two elliptic fixed points in the (β,l) plane. This range of k values is the domain of small angle scattering which corresponds to the regime of nonhyperbolic scattering ($E>10$) in our system with the Woods-Saxon potential. At $k=4$ the two elliptic points become hyperbolic. A similar critical point exists in the Woods-Saxon model where at $E\approx 10$ the scattering turns from nonhyperbolic to hyperbolic. We did not attempt to calculate this critical point with very high precision. After this critical point, the scattering in the two models is quite different. While in the TS model the invariant set in the k range $4<k<\pi R/D$ is trivial (it consists of two points only), in the Woods-Saxon model we observe nontrivial chaotic scattering in the energy range $E_f \lesssim E<10$. The new feature which the Woods-Saxon potential introduces is the existence of nontrivial chaotic scattering in the channeling regime in which a scattering trajectory going upwards (downwards) will never turn around and *scatter anew* from a scattering potential below (above) from which it came in the first place. In contrast to the TS model where the invariant set in the channeling regime is trivial, in the Woods-Saxon case this regime is characterized by two nontrivial dynamically decoupled chaotic invariant sets.

At $k=\pi R/D$ a bifurcation occurs in the TS model after which two invariant sets emerge which are dynamically coupled. In our case, before the heteroclinic collision, the two invariant sets are also dynamically decoupled. But in contrast to the TS model they are nontrivial Cantor sets. At a bifurcation they collide and form a single dynamically coupled set. This is the major new feature which is introduced by going from the linear deflection function model to the Woods-Saxon model, i.e., a model with realistic scatterers.

The existence of a nontrivial channeling regime is also apparent from Fig. 7(a), where the smooth structure in the scattering function originates from scattering off the entry disk, i.e., it reflects the shape of the single-disk scattering function $\theta(l)$. This function, as expected, is point symmetric around $l=0$ and $\beta_{\text{out}}=\beta_{\text{in}}$ ($=2.55$). It goes to zero, as expected, at $l=-l_{\max}=-4.4$, so $\beta_{\text{out}}=\beta_{\text{in}}=2.55$ at $-l_{\max}$. At $l_{\max}=4.4$ it deviates from zero since a particle can scatter once more from the potential immediately above. With this information, Fig. 7(a) shows that at $E=5$, we have essentially trivial one-(two-) disk scattering for $l>0$. For $l<0$, on the other hand, we see the complicated structures pointed out already in Sec. III which indicate the presence of chaotic scattering. Therefore, Fig. 7(a) clearly shows that at $E=5$ we have nontrivial chaotic scattering in the channeling regime. This result is a necessary condition for the major new phenomenon reported in this paper, namely, the occurrence of a crisis in chaotic scattering. Chaotic channeling provides the two dynamically decoupled sets which merge when crisis occurs.

ACKNOWLEDGMENTS

We thank I. Kan for suggesting one-dimensional models and R. Blümel for valuable discussions. This work was supported by the Department of Energy (Office of Scientific Computing, Office of Energy Research).

[1] M. C. Gutzwiller, Physica D **7**, 341 (1983); D. W. Noid, S. Gray, and S. A. Rice, J. Chem. Phys. **84**, 2649 (1986); C. Jung, J. Phys. A **19**, 1345 (1986); M. Hénon, Icarus **66**, 536 (1986); Physica D **33**, 132 (1988); B. Eckhardt and H. Aref, Trans. R. Soc. London Ser. A **326**, 655 (1988); B. Eckhardt, Europhys. Lett. **61**, 329 (1988); P. Gaspard and S. A. Rice, J. Chem. Phys. **90**, 2225 (1989); Z. Kovács and T. Tél, Phys. Rev. Lett. **64**, 1617 (1990); Y. C. Lai and C. Grebogi, Int. J. Bif. Chaos **1**, 667 (1991).

[2] S. Bleher, E. Ott, and C. Grebogi, Phys. Rev. Lett. **63**, 919 (1989); S. Bleher, C. Grebogi, and E. Ott, Physica D **46**, 87 (1990).

[3] M. Ding, C. Grebogi, E. Ott, and J. A. Yorke, Phys. Rev. A **42**, 7025 (1990).

[4] M. Ding, C. Grebogi, E. Ott, and J. A. Yorke, Phys. Lett. A **153**, 21 (1991).

[5] G. Troll and U. Smilansky, Physica D **35**, 34 (1989).

[6] G. Troll, Physica D **50**, 276 (1991).

[7] C. Grebogi, E. Ott, and J. A. Yorke, Phys. Rev. Lett. **48**, 1507 (1982); Physica D **7**, 181 (1983); C. Grebogi, E. Ott, F. Romeiras, and J. A. Yorke, Phys. Rev. A **36**, 5365 (1987); Y. C. Lai, C. Grebogi, and J. A. Yorke, in *Applied Chaos,* EPRI Workshop on Applications of Chaos, edited by J. H. Kim and J. Stringer (Wiley, New York, 1992), pp. 441–455.

[8] Y. C. Lai, C. Grebogi, R. Blümel, and I. Kan, Phys. Rev. Lett. **71**, 2212 (1993).

[9] J. D. Farmer, E. Ott, and J. A. Yorke, Physica D **7**, 153 (1983).

[10] C. Grebogi, S. W. McDonald, E. Ott, and J. A. Yorke, Phys. Lett. A **99**, 415 (1983); S. W. McDonald, C. Grebogi, E. Ott, and J. A. Yorke, Physica D **17**, 125 (1985).

[11] C. Grebogi, H. E. Nusse, E. Ott, and J. A. Yorke, in *Dynamical Systems,* edited by J. C. Alexander, Springer Lecture Notes in Mathematics Vol. 1342 (Springer-Verlag, New York, 1988), pp. 220–250.

[12] R. D. Woods and D. S. Saxon, Phys. Rev. **95**, 577 (1954).

[13] P. Ring and P. Schuck, *The Nuclear Many-Body Problem* (Springer-Verlag, New York, 1980).

[14] Y. C. Lai, R. Blümel, E. Ott, and C. Grebogi, Phys. Rev. Lett. **68**, 3491 (1992).